SACLANTCEN REPORT
serial no: SR- 347

SACLANT UNDERSEA RESEARCH CENTRE REPORT

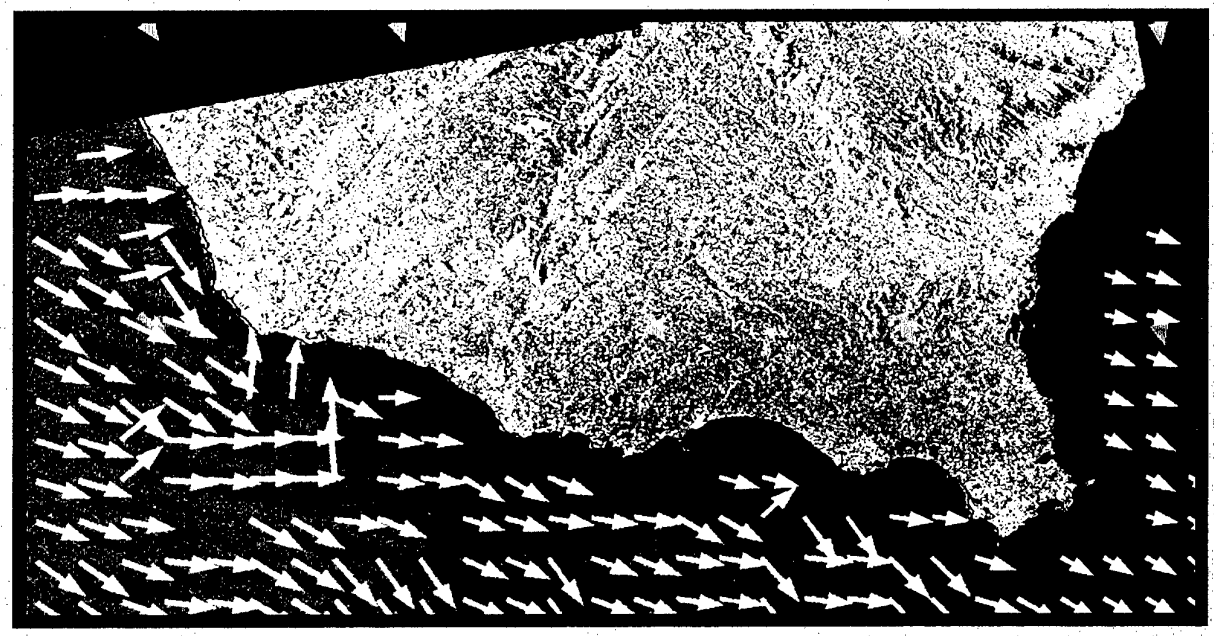

NORTH ATLANTIC TREATY ORGANIZATION ORGANISATION DU TRAITE DE L'ATLANTIQUE NORD

High resolution wind mapping with RADARSAT SAR imagery

Farid Askari, Serge Scevenels

The content of this document pertains to
work performed under Project 01-B of the
SACLANTCEN Programme of Work.
The document has been approved for
release by The Director, SACLANTCEN.

Jan L. Spoelstra
Director

intentionally blank page

High resolution wind mapping with RADARSAT SAR imagery

Farid Askari, Serge Scevenels

Executive Summary: Ocean surface winds affect many aspects of military operations in the littoral environment. To meet the requirements for more detailed characterization of wind fields at smaller spatial scales, new and evolving sensor concepts are needed to augment traditional data collection and prediction methods. This report focuses on high-resolution wind mapping using RADARSAT synthetic aperture radar (SAR) imagery, and constructing detailed descriptions of the wind field through synergistic use of multi-sensor information. For support of military operations in denied regions, operational commanders can construct high resolution pictures of the wind field by combining coarse resolution satellite observations and numerical model outputs with high-resolution SAR imagery. For operational use, however, the largest obstacles to overcome for SAR are the temporal resolution and timeliness of data delivery.

intentionally blank page

High resolution wind mapping with RADARSAT SAR imagery

Farid Askari, Serge Scevenels

Abstract: This article assesses the capabilities of RADARSAT SAR imagery for high-resolution wind mapping. The mapping technique couples a scatterometer model function with two-dimensional image analysis and other fusion techniques for inverting the SAR back-scattering cross-sections into wind vectors. The SAR-derived results are compared with shipboard *in situ* measurements, coarse resolution winds derived from the coupled ocean atmosphere prediction system (COAMPS) model, special sensor microwave imager (SSM/I) and QUICKSCAT satellite measurements. The sensor-to-sensor comparisons show good overall agreement. The largest discrepancies are associated with measurements from the SCANSAR imaging mode, where antenna calibration is a suspect.

Keywords: Keywords: wind retrieval, scatterometry, RADARSAT

Contents

1
Introduction

Spaceborne synthetic aperture radar (SAR) is a key sensor for denied-area surveillance and environmental monitoring, owing to its all-weather, day-night, and high resolution imaging capabilities. Advances in aperture synthesis, electronic beam-stearing techniques and multi-beam signal processing have paved the way for obtaining imagery with unprecedented resolution and spatial coverage for almost any coastal region on the globe. More recently the potential role of SAR for littoral zone monitoring has been exemplified by SAR's ability in diagnosing atmospheric boundary layer processes and resolving wind variations on the ocean surface. Although SAR was not originally conceived as a meteorological and wind-mapping sensor, it's newly discovered capability has sparked new opportunities for littoral zone environmental assessment. In response to the operational commanders demands for more detailed characterisation of the battle-space environment on smaller spatial and temporal scales, the modelling community has made significant progress in constructing rapidly relocatable, site-specific, three-dimensional, nestable models. However, lack of adequate observational data of important variables (winds, waves) at scales commensurate with model resolutions have hampered model performance. Marvellous synergy has occurred between regional or large-scale atmospheric circulation models and coarse resolution wind-mapping satellites (NASA/QUICKSCAT and European Remote Sensing ERS-2). Coastal prediction capabilities will be significantly enhanced if equivalent steps are taken for nesting high-resolution site-specific models with high-resolution SAR-derived wind fields. Short of conducting data-model assimilation, the two fields should be compared side-by-side. Independent views could prove valuable in interpretation and validation of both fields.

While the utility of SAR as a scientific instrument has been demonstrated successfully in many applications [1-4], its operational utility has progressed slowly because of several obstacles. First, spaceborne SAR have long revisit times (35 days for ERS, and 1-3 days for RADARSAT, depending on the latitude and choice of beam patterns) and second, the data delivery/processing times are slow compared to lifetime of the meteorological/oceanic phenomena. Even with the RADARSAT's shorter revisit times, several basic research and engineering issues need overcoming, before robust and reliable backscatter-to-wind inversion can be achieved. The engineering issues include inadequate system calibration, spacecraft attitude control and gain uncertainty resulting from time-dependent transmitted and received power [5]. The research issues involve difficulties in understanding/interpretation of km-scale image modulations associated with meteorological/oceanographic processes, and requirements for validation and field-testing of the newly proposed algorithms.

In spite of these complications, wind-inversion by the RADARSAT SAR appears to offer the greatest promise for high-resolution wind mapping in coastal areas where

measurements and techniques remain sparse. Our objective in this report is to assess the performance of RADARSAT SAR wind-inversion techniques. The significant contribution of the present work is the extensive comparison of the SAR-derived results with other wind products including shipboard *in situ* measurements, Coupled Ocean/Atmosphere Meso-scale Prediction System (COAMPS) model [6] outputs, and other satellite products.

In Section 2, we discuss the scatterometer model function, radiometric calibration, and wind direction problem associated with SAR wind inversion. RADARSAT-SAR products obtained with different processing techniques are compared to *in situ* measurements and other complimentary information are shown in Section 3. Discussions and conclusions are given in Section 4.

2
Methods

In this section we describe the scatterometer wind-retrieval techniques and discuss the calibration procedure. We summarize the characteristics of COAMPS winds and two spaceborne sensors, the QuickSCAT/SeaWinds and the special sensor microwave imager (SSM/I) which are used in our study for comparison and verification of SAR-winds.

2.1. SAR-SCATTEROMETRY

The first scatterometer was flown onboard the NASA/SKYLAB in 1973. From very early on it was recognized that a correlation existed between the backscattering signal produced by the short capillaries and gravity waves and the surface wind stress. In order to explain the relationships between the wind vector and the radar back-scattering cross-section and other parameters including radar frequency, polarization, incidence angle and look direction, several empirical and physically-based scatterometer model functions have been developed in recent years [7-8]. The empirical model function which relates the normalized radar cross-section (NRCS) σ_0 (for transmit and receive polarization p) to wind speed has a general form:

$$\sigma_0{}^{p} = aU^{\gamma}(1 + b\cos\phi + c\cos 2\phi) \tag{1}$$

where U is the wind speed, ϕ is the wind direction relative to the look direction of the radar antenna, and a, b, c, and γ are empirically derived coefficients that are dependent on radar frequency, polarization and incidence angle. The most widely used model for describing the mean background at C-band is the CMOD4 algorithm [4]:

$$\sigma_0 = b_0\left[1 + b_1\cos\phi + b_3\tanh(b_2)\cos(2\phi)\right]^{.6} \tag{2}$$

$$b_0 = \delta x\begin{Bmatrix} 10^{\alpha}\, if, U+\beta \le 0 \\ 10^{\alpha}(U+\beta)^{\gamma}\, if, 0 < U+\beta \le 5 \\ 10^{\alpha+0.3125\gamma\sqrt{U+\beta}}\, if, 5 < U+\beta \end{Bmatrix}$$

where,

$$\alpha = c_1 + c_2 P_1 + c_3 P_2, \beta = c_4 + c_5 P_1 + c_6 P_2, \gamma = c_7 + c_8 P_1 + c_9 P_2$$
$$b_1 = c_{10} + c_{11} U + \left[\tanh(2.5(P_1 + 0.35)) - 0.61(P_1 + 0.35)\right](c_{12} + c_{13} U)$$
$$b_2 = c_{14} + c_{15}(1 + P_1)U$$
$$b_3 = 0.42(1 + c_{16}(3 + P_1)(U - 10))$$
$$P_1 = (\theta - 40)/25, P_2 = (3P_1^2 - 1)/2$$

This algorithm has been extensively tested using data from the ERS-1/2 satellites. The SAR/scatterometer instruments on board the ERS operate in the vertically polarized transmit/receive (VV) configuration, whereas the RADARSAT SAR operate horizontally polarized transmit/receive (HH) configuration. Thus a modified version of CMOD4 algorithm has been proposed [1] when using RADARSAT data. The model coverts the HH scattering to VV using:

$$\sigma_0^H = \frac{\left(1 + \alpha \tan^2 \theta\right)^2}{\left(1 + 2\tan^2 \theta\right)^2} \sigma_0^V (U, \theta, \phi) \tag{3}$$

In equation 3, U, θ, ϕ are respectively, the wind speed, incidence angle, and azimuth angle of the radar with respect to the wind direction, and σ_0^H and σ_0^V are the HH and VV radar cross-sections. Equation 3 is used to invert the SAR cross-sections into wind speeds.

2.2 RADIOMETRIC CALIBRATION OF RADARSAT/SAR IMAGERY

The first step involved in backscatter-to-wind-speed inversion is the radiometric calibration of the SAR imagery. The RAW SAR signal contains unprocessed radar video baseband data in complex in-phase and quadrature signal (I and Q) format as they are recorded by the spacecraft. The pixel in an image is represented by a single integer (8 or 16 bits) using the magnitude of the complex number [9]:

$$\mathrm{DNj} = \sqrt{I^2 + Q^2} \tag{4}$$

In 4, DNj is the digital number that represents the magnitude of the jth pixel from the beginning of a range line in the detected image data, then the corresponding value of the brightness, β_j^0, for the pixel is given by:

$$\beta_j^0 = 10 * \log 10[(DNj^2 + A3)/A2j]dB \tag{5}$$

where A2j and A3 are scaling and offset coefficients. Finally the relationship between radar brightness (β_j^0) and radar backscatter coefficient (σ_0) is given by [9]:

$$\sigma_j^0 = \beta_j^0 + 10 * \log 10(\sin Ij) dB \tag{6}$$

where, *Ij* is the incidence angle at the jth range pixel.

RADARSAT employs electronic beam-steering (Fig. 1) for in-flight modification of incidence angles and beam modes [9]. Here we assess the capabilities of the SCANSAR and STANDARD beam modes for wind-retrieval. In the SCANSAR – Narrow imaging mode, between two to three single beams are employed and combined during data collection. The beams are selected sequentially, thereby creating a wider swath (up to 300 km) than is possible from a single beam. The wide swath coverage, however, comes at the expense of reduced spatial resolution over a single beam. The nominal range and azimuth resolutions are 50 × 50 m respectively. In the STANDARD mode there are seven beam positions. Each beam covers a minimum ground swath of 100 km. The azimuth resolution is the same for all beam positions, 27 m, whereas the range resolution (25 m nominally) changes from beam to beam. The principal advantage of STANDARD beam over the SCANSAR mode is its radiometric image quality, where pixels are represented as 16-bit gray levels. The STANDARD beam mode also offers more flexibility in the choice of incidence angles. The final images are re-sampled to 25 m per pixel in both directions for SCANSAR mode, with intensity values ranging between 0 to 255 digital counts (8-bit), and 12.5 m for STANDARD mode with intensity values ranging between 0 to 65536 digital counts (16-bit).

2.3 WIND DIRECTION PROBLEM

Conventional scatterometer techniques obtain the oceanic wind vector by inverting a model function that relies on the "Bragg resonant" reflections from the slopes of wind-generated gravity-capillary short waves. As seen in Eq. (1) because the backscattering is anisotropic, wind direction must be retrieved using multiple azimuthal views supplied from a rotating antenna, or from multiple fan-beam antennas mounted at different orientations with respect to the satellite ground track. SAR can be utilized as a high-resolution imaging scatterometer because the image intensity is proportional to the back-scattered power from the sea surface, which is a strong function of the small-scale surface wave spectral density, which in turn is related to the wind stress. For SAR scatterometry, however, there is one fundamental problem: SAR views the ocean surface only at a single azimuth angle (or the line-of-sight component of the wind), while the inversion process requires *a priori* knowledge of the angle between the wind and the antenna.

If the imagery contains surface expressions of wind-generated phenomenon such as atmospheric boundary layer wind rolls, wind-waves or island-wakes, the wind-antenna

angle (or wind direction) can be inferred from the SAR imagery using 2D Fourier image analysis techniques. In the absence of such information, other approaches involving optimum blending of model functions with ancillary information must be utilized. While considerable progress has been made to arrive at this information *a priori*, no satisfactory solution has yet been proposed that works under all imaging conditions.

The use of atmospheric general circulation model (GCM) outputs as inputs to the SAR-wind-mapping procedure have been proposed [1]. As will be shown here, this approach provides a reasonable solution to high resolution wind mapping using low resolution wind directions, provided the time lag between the model outputs and SAR observations is small.

COMPARISON PRODUCTS

2.4. COAMPS WINDS

For the Mediterranean, the wind fields derived from COAMPS are received at SACLANTCEN *via* FTP from the Fleet Numerical Meteorological and Oceanography Center (FNMOC) in Monterey, California every twelve hours. COAMPS is a analysis-nowcast and short-term forecast (up to 48 hours) tool which assimilates into a 27 km numerical model observations from aircraft, rawinsondes, and satellites with first-guess fields to generate nowcast-forecast of meteorological fields [6]. The system utilizes nested grids to achieve high-resolution for a given region, and uses the global fields from the Navy Operational Global Atmospheric Prediction System (NOGAPS) as boundary conditions.

2.5 QUICKSCAT/SEAWINDS

Wind vector measurements from the QuickSCAT on board the SeaWinds satellite (NASA's Quick Scatterometer) provide for another comparative data source. Currently SeaWinds is the only satellite that provides near global coverage (90% of Earth's surface) of the oceanic wind-vector in a single day. The wide spatial coverage (1800 km swath) is made possible by combining a high orbital inclination (98.6°) with a rotating antenna. The antenna has two spot beams that sweep the surface in a circular pattern as the satellite moves in the along-track direction. QuickSCAT operates at Ku-band (13.4 GHz) and has a 25 km resolution cell. The instrument specifications call for measurements of winds between 3 to 20 m/s with an accuracy of 2 m/s, and direction accuracy of 20 degrees. The QuickSCAT project is managed by the JPL/NASA. High-quality research data products are produced and distributed by JPL to the science community through the Physical Oceanography Distribute Active Archive Center (PODAAC) web-site (http://podac.jpl.nasa.gov). The QuickSCAT Level 3 data files are received at SACLANTCEN *via* FTP from JPL/PODAAC in Hierarchical Data Format

(HDF). The Level 3 data are considered science data products where backscatter-to-wind calibration and navigation have been performed. Each HDF file contains data from the ascending and descending passes over the entire globe, where the east and west components of the wind vector, latitude and longitude and rain flags are tabulated as non-gridded fields [11].

2.6 SSM/I WIND-RETRIEVAL

The special sensor microwave imager (SSM/I) measures the ocean surface wind speed via measurements of sea surface microwave emissions. Currently four SSM/I sensors operate on board the DMSP (F10-F14) satellites, which collectively provide good temporal-spatial coverage of critical environmental parameters over the world oceans.

The wind retrieval method uses a linear combination of measured SSM/I brightness temperatures that vary with frequency and polarization. Microwave energy emitted and measured as brightness temperature from the ocean surface is related to the wave structure and foam coverage, which in turn is related to the surface winds. The SSM/I accuracy specification for wind speed retrieval is ± 2 m/s over the range of 3-25 m/s. The SSM/I is a seven-channel four-frequency radiometer with frequencies centered at 19.35, 22.235, 37.0, and 85.5 GHz. All frequencies are received in vertical (V) and horizontal (H) polarization, except for the 22 GHz, which is received only in vertical polarization. The SSM/I has a conical scan with a swath width of 1400 km. The Effective-Fields-of-View (EFOV) for the four channels are 43 × 60, 40 × 50, 28 × 37, and 13 × 15 km, respectively [12].

3
Results

Our objective is to describe a methodology for extracting high-resolution wind vector from SAR imagery. In this section we show examples of SAR imagery where signatures of atmospherically-induced phenomenon allow for retrieval of the complete wind field. Following that we show another situation where the inversion process calls for the use of ancillary information. The section ends with a comparison of SAR-derived winds with *in situ* observations, numerical model forecasts and other satellite observations.

3.1 HIGH-RESOLUTION WINDS FROM RADARSAT

The RADARSAT images (Figs. 2-6) were acquired over the southeastern coast of Sicily near the Malta Plateau. The images for March 3 and 10 were collected in SCANSAR imaging mode, and for April 29, 30, May 4 in STANDARD mode. The images collected on 3 March, 29 and 30 April contain the most visibly obvious expressions of atmospherically-generated phenomenon such as boundary layer wind rolls, wind-generated gravity waves, lee-waves originating from topographic influences, and island-generated wakes.

The March 3 SAR image (Fig. 2) provides the opportunity for examining the details of the wind retrieval procedure, as it contains both signatures of atmospheric boundary layer rolls and wind-generated gravity waves. In SAR imagery, wind rolls are manifested as linear roughness features with horizontal spacing that vary typically between 1 to 8 km, although 20 km spacing has been reported [13]. Atmospheric boundary layer rolls are helical circulation patterns which are superimposed on the mean wind field [14]. Rolls can be generated either by thermal instability when the layer is heated from below or cooled from above, or by dynamic instability (inflection point instability). The roll axis is oriented between the direction of the mean surface wind and the geostrophic wind above the boundary layer. Hence roll orientations can be used for inferring wind directions [15]. In general, it appears (from observation and theory) that on the average roll orientation can estimate wind direction to within 15°. Alternatively, wind-wave propagation direction can be used (in the absence of swell) to derive wind direction. In the spatial frequency Fourier domain, wind-rolls are mapped into the low-frequency (km-scale) components, whereas wind-waves are mapped in to the high-frequency components (m-scale).

For wind inversion, subsequent to calibration and geo-referencing, we divide the SAR image into a series of 5 × 5 km blocks. For each block the mean intensity and a low-order polynomial trend are computed and subtracted from the individual pixel values.

The 2D-FFT spectra are computed and smoothed using a 2-D Gaussian filter (Figs. 7-8). The orientation of the 2D-spectrum is computed using the slope of the line that connects the spectral peaks falling within an annulus defined by a lower wave-length of pixel-spacing × 4, and a higher wave-length of pixel-spacing × 40. For wind-waves the interval corresponds to 50m and 1 km (Fig. 7), and for wind rolls to 1 and 4 km (Fig. 8). Because the wind rolls axes are nearly parallel to the wind direction, the FFT-derived angles require a 90° rotation for assigning wind direction (with 180° ambiguity). For wind waves no rotation is necessary.

With the wind direction estimates and radar cross-section (σ_0) measurements in hand, we invert the back-scattering values via Eq. (3), and arrive at the wind speed that is most consistent with the measured wind direction and σ_0 values. The procedure is repeated over every cell until a complete wind vector map is produced. Using information from the individual 5 × 5 km blocks, however, results in a somewhat noisy map. To reduce the noise a uniformity test is applied. The uniformity test compares the 5 × 5 km 2D-FFT directional spectra with spectra computed over a larger 20 × 20 km domain. If the high-resolution directions are within $\pm 90^\circ$ of the low-resolution directions, they remain the same, otherwise they are replaced by the low-resolution directions.

The high frequency SAR wave number spectra derived from 20 × 20 km blocks are shown in Fig. 9. The radial distance from the spectral center is linearly proportional to reciprocal ocean wavelength, with the inner radius corresponding to 500 m and the outer radius to 100 m. Note two peaks aligned second and fourth quadrants, which represent 200 m waves propagating (with 180° ambiguity) in the direction of dominant wind. The low frequency (20 × 20 km) spectra show (Fig. 10) peaks between 2000 to 2500 m wavelength in the first and third quadrants. The resulting smoothed wind-vector maps using both high and low frequency components show a predominantly southeastward wind direction (Figs. 11-12). We note that the wave-generated directions are rotated slightly (counterclockwise) with respect to the roll-generated directions. This is attributed to the fact that in addition to the 90° rotation of the FFT, we imposed a 13° rotation on the roll-orientation-to-surface-wind-direction computation as recommended in [10]. Theoretical calculations indicate rotations of 13°-15° to the left of the geostrophic wind for inflection point instability and parallel instability, respectively [10].

Using the procedure described above we generate wind vector maps for March 10, April 29, 30 and May 4 (Fig. 13-16). For March 10, April 30 and May 4 we exploit the wind-wave spectrum information. For April 29 the wind-roll spectrum is used for deriving the wind vectors

For May 4, because of the lack of any obvious features we utilize the COAMPS-wind-directions in the scatterometer wind retrieval. In Fig. 17 the COAMPS winds are interpolated down to the SAR cell size (5 km) using nearest neighbor approach. Because COAMPS predictions are produced every three hours, we choose the time that is closest to the SAR over pass.

3.2 COMPARATIVE WIND FIELDS

In Figures 11-16 we append the SAR-derived (white) wind vectors with the geo-referenced colour-coded wind vector fields derived from the R/V *Alliance,* COAMPS, and QuickSCAT. Figure 18 show the wind fields in the immediate vicinity of the R/V *Alliance*. Because the *Alliance* was continuously recording the winds, we select the surface winds corresponding to the time of the RADARSAT overpass. The time lag between RADARSAT overpass and other sensors, however, can vary from two to twelve hours. Obviously as the time lag increases we should expect decorrelation among sensors. The mean and variance for wind speeds and directions for different sensors are listed in Table 1.

A 2D-plot provides another means for illustrating the sensor-to-sensor comparisons, with the y-axis showing the wind speed (or wind direction) and the x-axis representing the different sensors (Fig. 19). The different curves correspond to wind information reported by individual sensors on a given day. We note that for March 3 and 10 images (both collected in SCANSAR mode) the SAR-derived wind speeds tend to be higher than other fields. The largest discrepancy in wind speed is associated with March 10 image which also shows high variability in wind direction. More than likely this is due to calibration and antenna pattern artifacts (more evident over land) which can generate spurious frequency components in the FFT analysis. For 4 May, all fields show low wind speeds.

4

Discussion and conclusions

Performance of RADARSAT wind-inversion techniques was assessed under a range of environmental conditions. As shown here and in other studies, when coherent wind-induced features appear in SAR imagery, wind vector retrieval becomes a routine procedure. When SAR imagery is devoid of such features, however, ancillary information from low-resolution numerical models (or QuickSCAT) must be utilized. The results obtained by the first method are clearly superior to the second method, because wind direction is inferred directly from the imagery *vs* from a model. From an operational perspective, however, where the goal is routine, global, near-real-time products, the first method becomes unreliable, as the prevalence of such features is inextricably linked to the thermal stability of the air-sea interface.

When comparing wind information derived from multiple sensors, due to each sensor/model's idiosyncrasies, the comparative fields should not be credited as "sea-truth" or "more-accurate" than the SAR-derived winds. The atmospheric wind speed at the sea surface spectrum spans a wide range of spatial and temporal frequencies and includes the effects of energy sources at the synoptic-scale, meso-scale, and micro-scale [15]. To obtain meaningful comparison of such a broad band signal, *in situ* observations must be averaged over scales corresponding as closely as possible to the SAR image area used in the wind speed estimate. For comparing fixed-position measurements from ships or buoys with remotely sensed winds, the "frozen turbulence" hypothesis is invoked, whereby the assumption that a time average can be substituted for a spatial average is made. Although some guidelines for averaging periods have been established for *in situ* validation of large-scale (20-30 km) scatterometer measurements, there are no well-defined rules for smaller resolution cells (1-5 km). For synoptic scale meteorological phenomenon, averaging periods range from 5 to 60 min. In addition to the space/time sampling issues, ship-measured winds are subject to flow distortions or ship blockage effects, biases due to variable mast heights, sporadic coverage, and navigational errors resulting from the relative motions of the ship, wind, and surface current velocities.

Another reminder is that the wind field at a particular point is often poorly represented by an average over many tens of kilometres, as portrayed by low-resolution satellite measurements and numerical models. We expect that many of the local inhomogeneities in the wind field arising from micro-bursts or oceanic frontal effects that are readily visible in SAR, will be "blurred" in the QUICKSCAT and SSM/I measurement due to the averaging of backscattering cross-sections over large foot prints.

Finally, the inclusion of the physics of Organized Large Eddies (OLE) in GCM models is essential when comparing SAR measurements with outputs of numerical GCM. As discussed by [16], GCM models generally have poor planetary boundary layer (PBL)

approximations, and without OLE's inclusions model/SAR comparisons become fruitless.

We can draw several conclusions from the work presented here:

- The broad-band nature of the wind speed spectrum and space/time sampling issues make comparison of multisensors difficult. For detailed quantitative analysis the observations must be collocated in space and time, and spatial/temporal decorrelation scales accurately known.
- In spite of the small sample size considered here, the SAR-derived winds showed good overall agreement and consistency with other wind products. The 10 March SCANSAR measurements was an exception where wind speeds were over predicted by a factor of two owing to calibration errors.
- Although the status of SAR scatterometry for measuring high-resolution winds is very promising, it is not yet fully established and further development is called for prior to routine generation of operational products.
- The SAR scatterometry method employs a model function that is capable of generating information over a 1-5 km spatial resolutions for winds between 2 to 20 m/s, with an accuracy of ± 2 m/s in wind speed and $\pm 15^{\circ}$ in wind direction. A notable weakness in the inversion technique is the need for *a priori* knowledge of the wind direction. In the absence of recognizable wind-induced structures, wind direction must be supplied from ancillary information, in which case the accuracy of results will depend on the accuracy of inputs.
- The application of SAR scatterometry holds the potential for estimating km-scale wind field all the way to the coastline for any region on the globe. This capability opens a new realm for coastal current and wave forecasting. Because of its imaging capability, SAR can diagnose geophysical processes (bathymetry, wave refraction, slicks) influencing spatial wind variability which may not be apparent in atmospheric numerical model outputs.
- Synergism between SAR scatterometry and high-resolution modelling would greatly facilitate verification studies. Emphasis should be placed on co-ordinating a vigorous campaign involving remote sensing measurements, high-resolution coupled atmospheric/oceanic models, and high-density observations from a network of coastal stations over an extended time period.
- The research shown here is a necessary prerequisite to data assimilation and validation studies. Currently, SAR surpasses all other sensors in terms of capability to document the spatial variability and morphological characteristics of the wind field. Even in the absence of assimilation, SAR's perspective on spatial variability would add important insight into model formulation and parameterization.

Table 1

Date	Alliance		QUICKSCAT					COAMPS					SSMI			SAR								
																WIND ROLLS				WIND WAVES				
	Wind dir	Wind sp	Time	Wind dir	Wind dir	Wind sp	Wind sp	Time	Wind dir	Wind dir	Wind sp	Wind sp	Time	Wind sp	Wind sp	Time	Wind Dir	Wind Dir	Wind sp	Wind sp	Wind Dir	Wind Dir	Wind sp	Wind sp
				Mean	Stdev	Mean	Stdev		Mean	Stdev	Mean	Stdev		Mean	Stdev		Mean	Stdev	Mean	Stdev	Mean	Stdev	Mean	Stdev
3-Mar	303	10.1	5:06	304	2	11.2	1	17:59	311	3.1	9.6	1.4	6:00	4.6	1.4	7:20	311	13.1	12.9	1.8	292	3.5	11.5	0.4
10-Mar	302	8.9	5:02	279	0.1	12	0.6	16:43	296	5.1	7	0.8	6:00	NV	NV	7:03	NV	NV	NV	NV	108	7.4	18.5	2.5
29-Apr	297	10.3	16:59	284	0.2	18.9	0.45	17:26	310	10.2	7.2	1.9	18:00	11.8	6	20:52	293	15	10.4	1.7	244	34.8	9.7	1.3
30-Apr	320	6.1	5:14	305	17.5	2.8	1.2	17:03	314	7.5	7.1	0.5	6:00	9.1	1.7	6:58	18	0	8.6	1.6	303	15.8	5.5	0.6
4-May	324	3	4:58	326	237.3	2	1.1	17:02	38	10.2	3.6	0.2	6:00	NV	NV	NV	330	16.8	3	0.2	317	6.4	3.3	0.4

Acknowledgements

The authors thank Dan Hutt from DREA, Canada for providing the RADARSAT SAR imagery, Martin Siderius and Charles Holland from SACLANTCEN for providing *in situ* information from the BOUNDARY-2000 and MAPEX-2000 experiments, and Rich Signell for reviewing the report. The QuikSCAT science data product were obtained from the NASA Physical Oceanography Distributed Active Archive Centre at the Jet Propulsion Laboratory / California Institute of Technology.

References

[1] Thompson, D.R., Beal, R.C. Mapping high-resolution wind fields using synthetic aperture radar. *JHU/APL Technical Digest*, **21**, 2000:58-67.

[2] Horstmann, J., Lehner, S., Koch, W., Tonboe, R. Computation of wind vectors over the ocean using spaceborne synthetic aperture radar. *JHU/APL Technical Digest*, **21**, 2000:100-107.

[3] Mourad, P.D., Thompson, D.R., Vandemark, D.C. Extracting fine-scale winds from synthetic aperture radar images of the ocean surface. *JHU/APL Technical Digest*, **21**, 2000:108-115.

[4] Stoffelen, A., Anderson, D.L.T. ERS-1 scatterometer data characteristics and wind retrieval skill. Proc. First ERS-1 Symp., Noordwijk, The Netherlands, ESA SP-359, 1993.

[5] Beal, R.C. Toward an international storm watch using wide swath SAR. *JHU/APL Technical Digest*, **21**, 2000:12-20.

[6] Hodur, R.M. The Naval Research Laboratory's Coupled Ocean/Atmospheric Mesoscale Prediction System. *Monthly Weather Review*, **125**, 1997:1414-1430.

[7] Plant, W.J. A two-scale model of short wind-generated waves and scatterometry, *Journal of Geophysical Research*, **91**, 1986:10,735-10,749.

[8] Schroeder, L.C., Boggs, D.H., Dome, G., *et al.* The between wind vector and normalized radar cross-section used to derive SEASAT satellite scatterometer winds. *Journal of Geophysical Research*, **87**, 1982:3318-3336.

[9] RADARSAT, data products and specifications, RSI-GS-026. RADARSAT International, Richmond, B.C., Canada, 1997.

[10] Wackerman, C.C., Rufenach, C.L., Shuchman, R.A., Johannessen, J.A., Davidson, K.L. Wind vector retrieval using ERS-1 synthetic aperture radar imagery. *IEEE Transactions on Geoscience and Remote Sensing*, **34**, 1996:1343-1352.

[11] Dunbar, R.S. *et al.* QuickSCAT Science Data Product User's Manual, Version 1, JPL Document D-18053, Jet Propulsion Laboratory, Pasadena, CA., 2000.

[12] Colton, M., Poe, G. Intersensor calibration of DMSP SSM/I. *IEEE Transactions on Geoscience and Remote Sensing*, pp 178-185, 1999.

[13] Etling, D., Brown, R.A Roll vortices in the planetary boundary layer: A review. *Boundary-Layer Meteorology*, **65**, 1993:215-248.

[14] Alpers, W., Brummer, B. Amospheric boundary layer rolls observed by the synthetic aperture radar abroad the ERS-1 satellite. *Journal of Geophysical Research*, 1994:12,613-12,621.

[15] Young, G.S., SAR signatures of the marine atmospheric boundary layer: implications for numerical forecasting. *JHU/APL Technical Digest*, **21**, 2000:27-32.

[16] Brown, R.A, Serendipity in the use of satellite scatterometer, SAR, and other sensor data. *JHU/APL Technical Digest*, **21**, 2000:21-26.

intentionally blank page

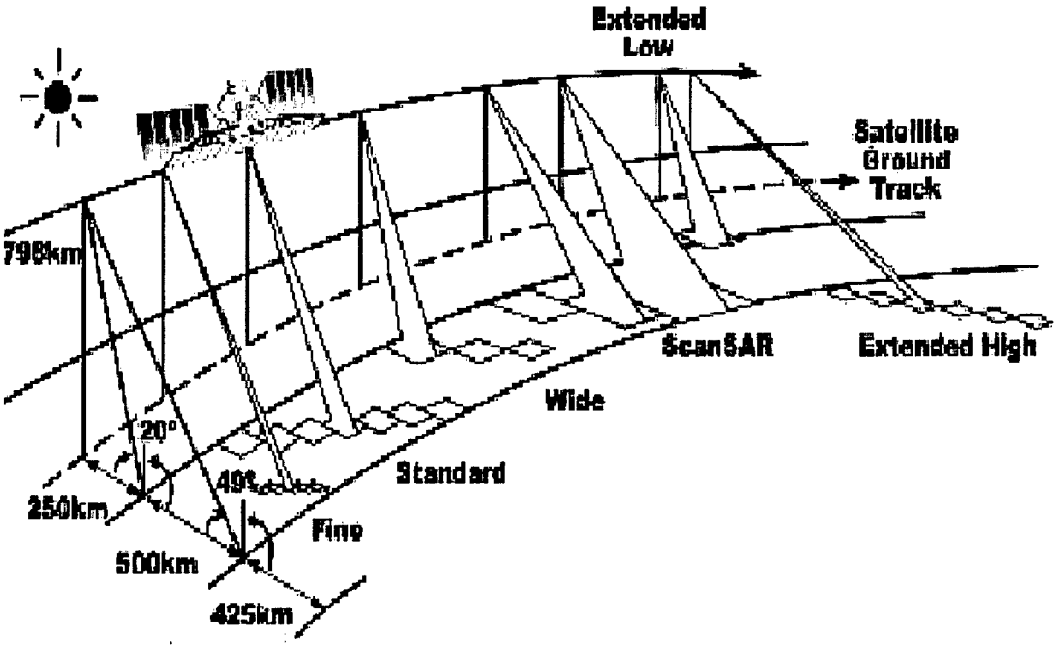

Figure 1 *RADARSAT SAR imaging geometry and beam modes. The STANDARD and SCANSAR beam modes are pertinent to this study.*

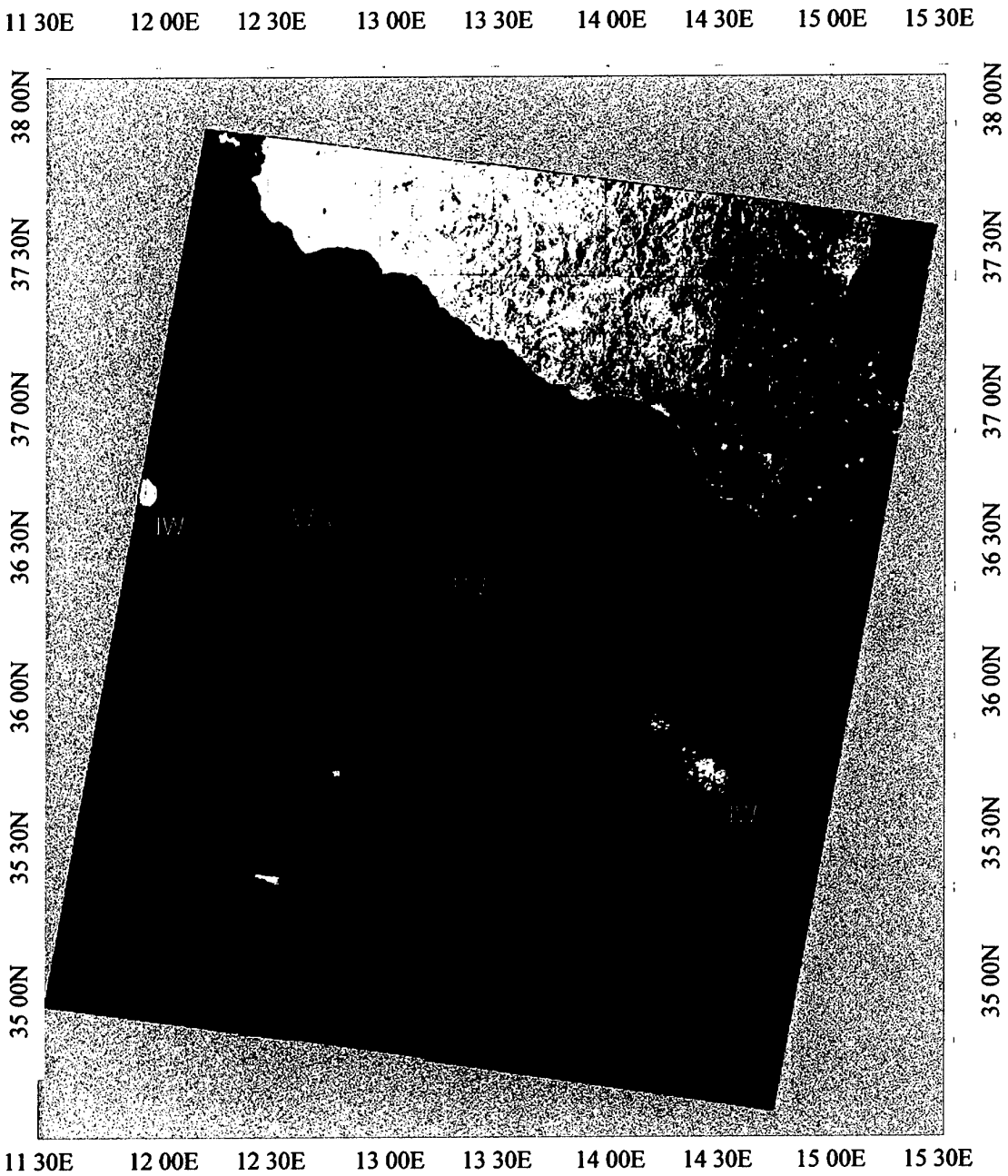

Figure 2 *RADARSAT SCAN-SAR image for March 3, 2000. The symbols IW, WR, LW refer to Island Wake, Wind Rolls, and Lee waves, respectively.*

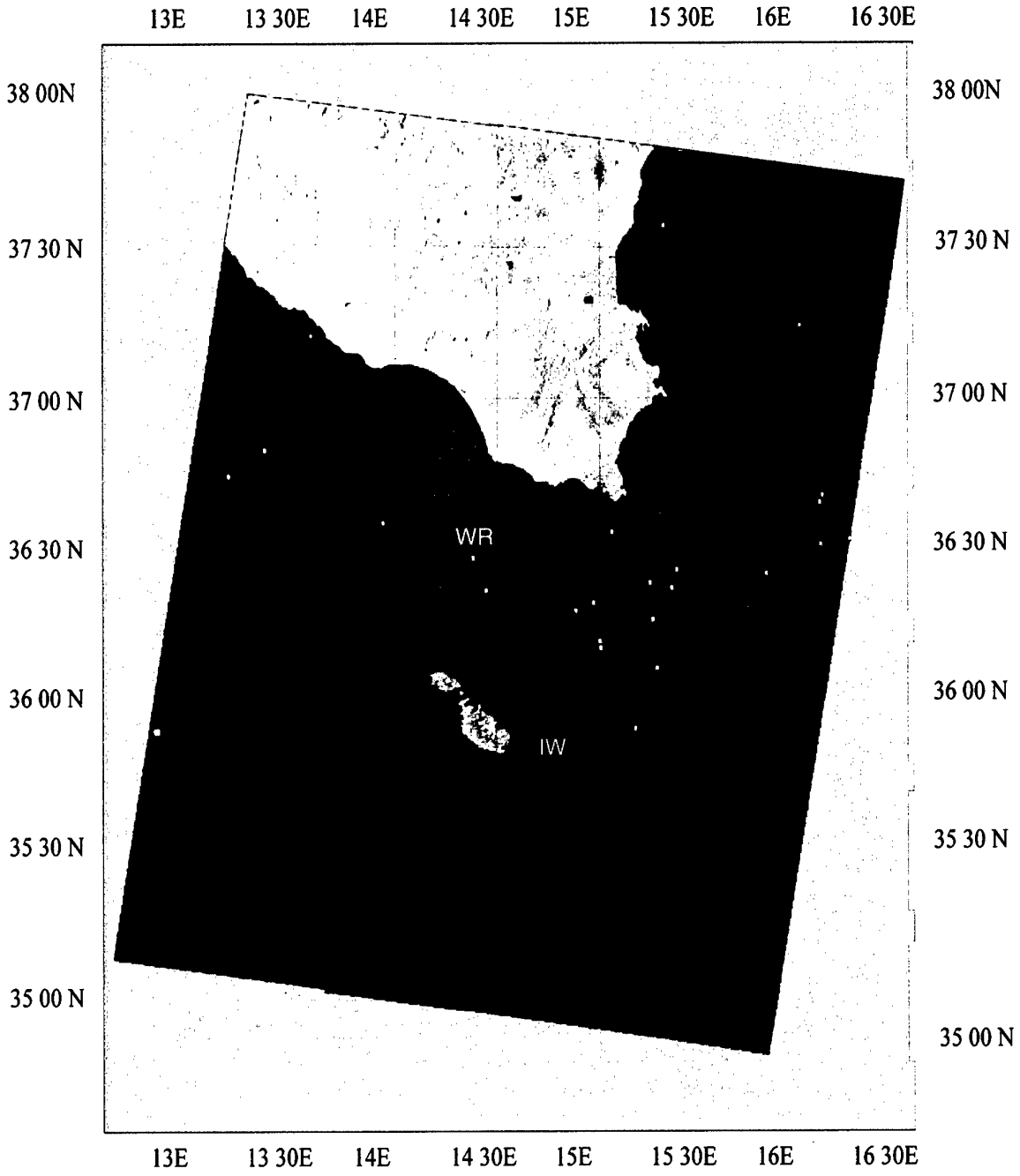

Figure 3 *RADARSAT SCAN-SAR image for March 10, 2000. The symbols IW, WR, refer to Island Wake, Wind Rolls, respectively.*

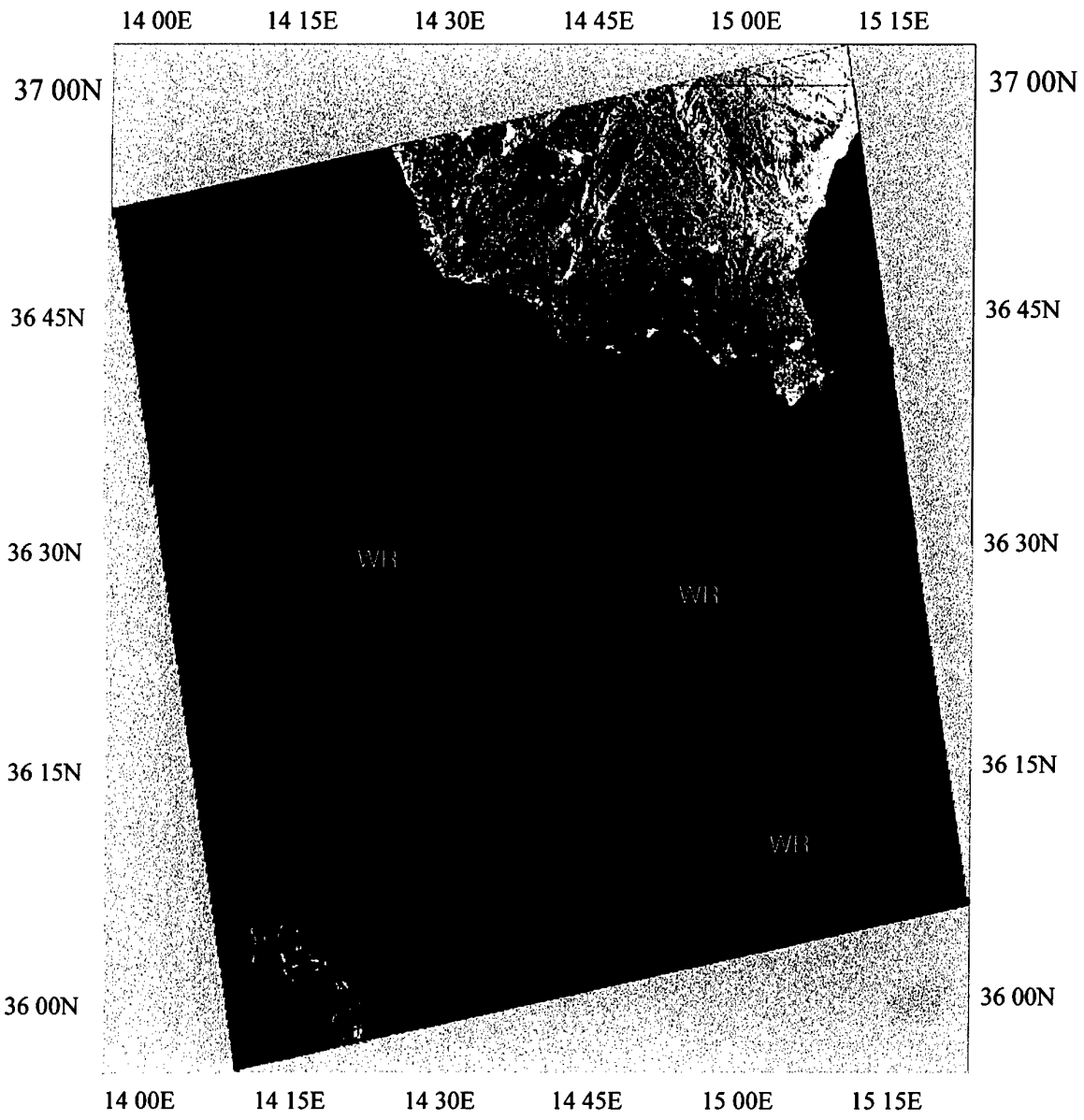

Figure 4 *RADARSAT STANDARD-SAR image for April 29, 2000. The symbol IW refers to Wind Rolls.*

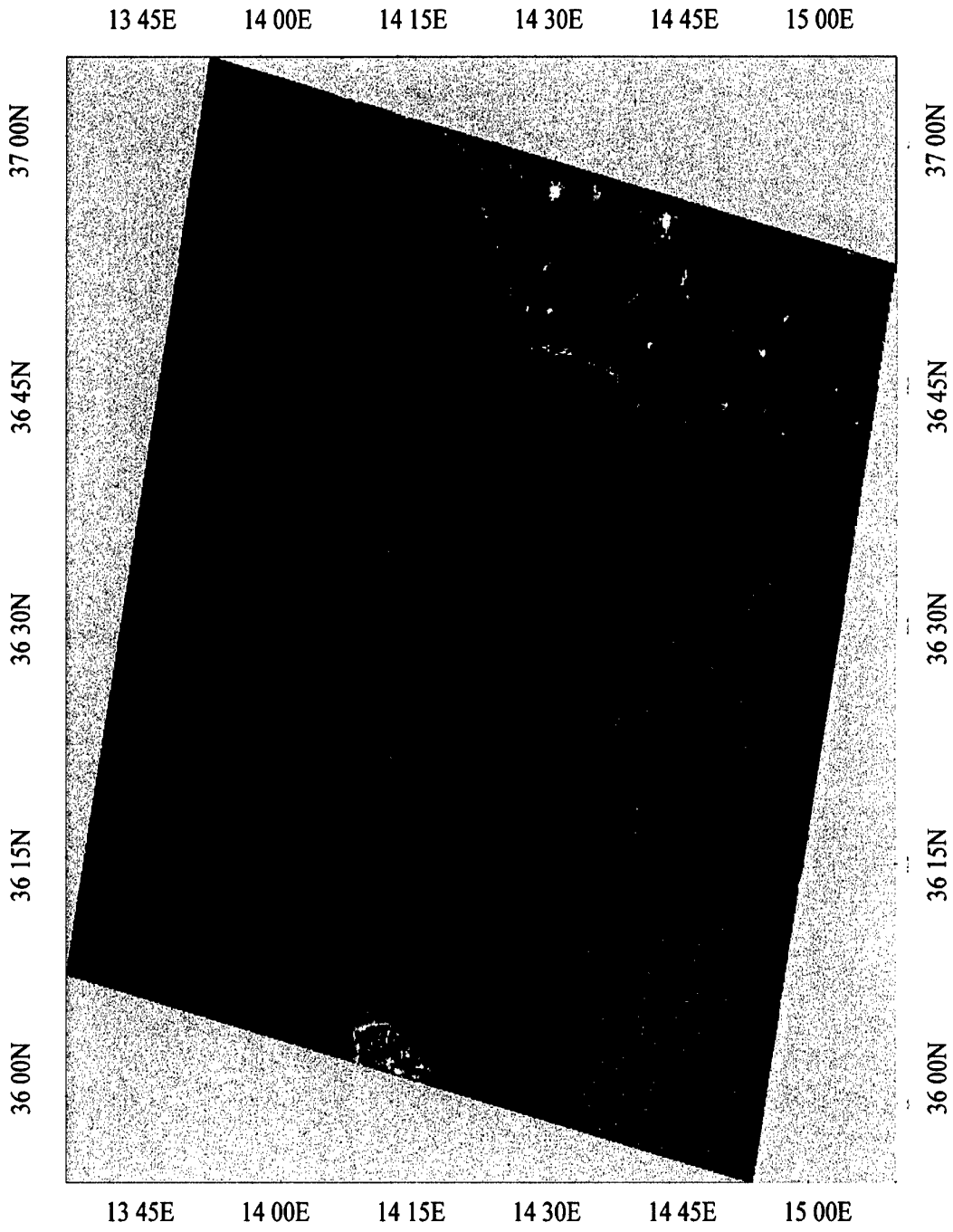

Figure 5 *RADARSAT STANDARD-SAR image for April 30, 2000.*

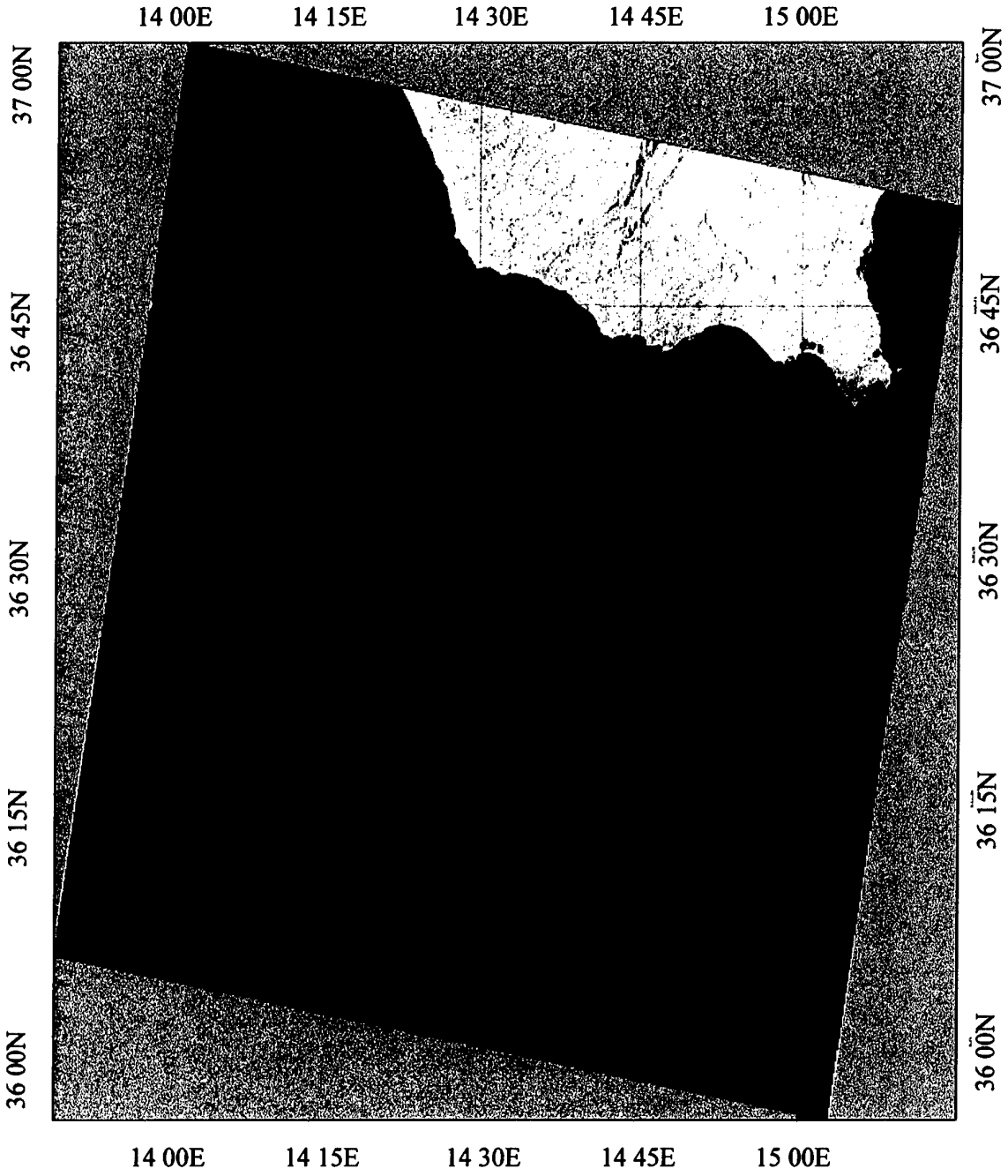

Figure 6 *RADARSAT STANDARD-SAR image for May 4, 2000.*

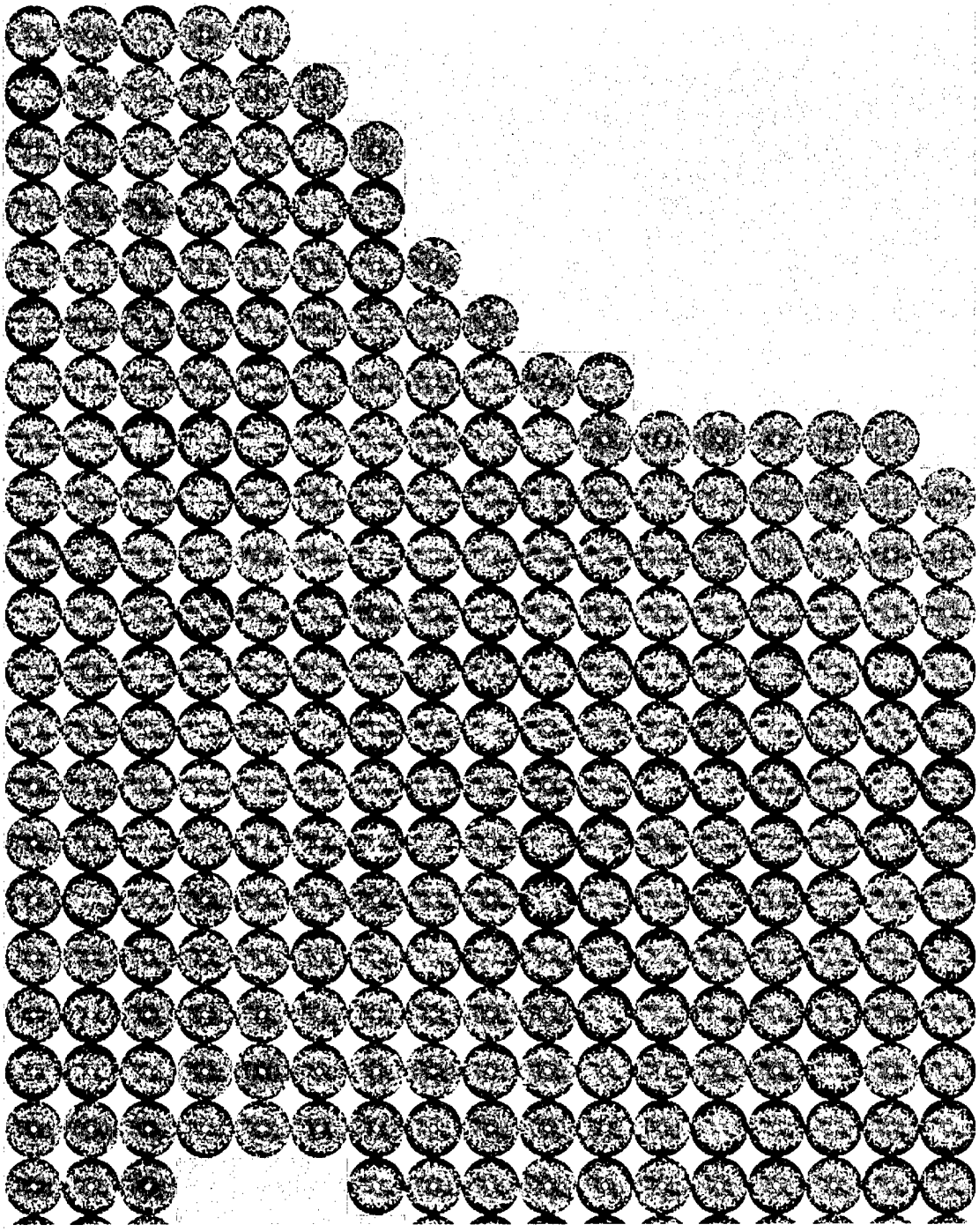

Figure 7 *High wave-number 2D-FFT spectra computed using 5 × 5 km blocks for March 3. The blue-green coloured peaks correspond to 200 m surface gravity waves.*

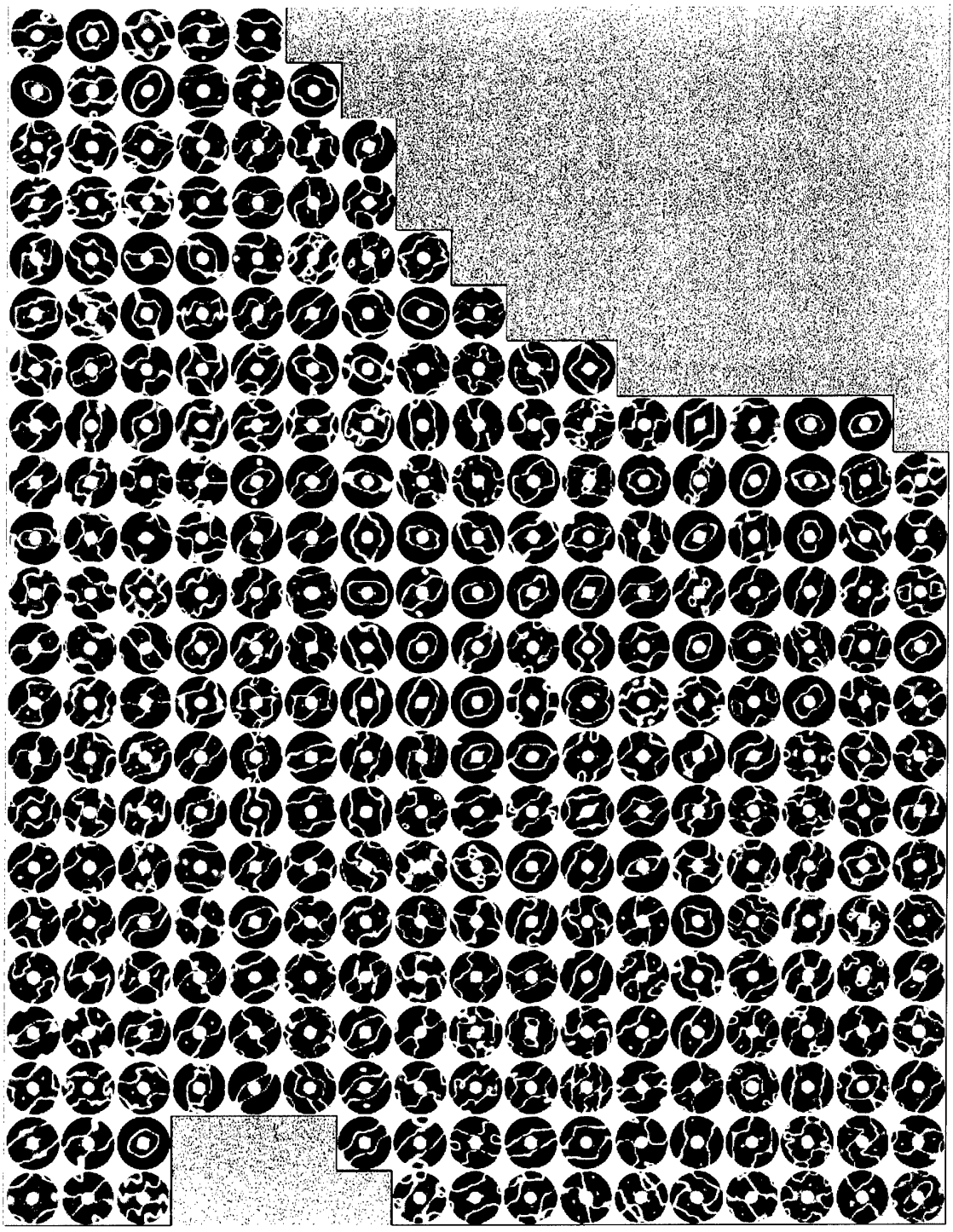

Figure 8 *Low wave-number 2D-FFT spectra computed using 5 × 5 km blocks for March 3. The blue-purple coloured peaks correspond to 2 k m wind-rolls.*

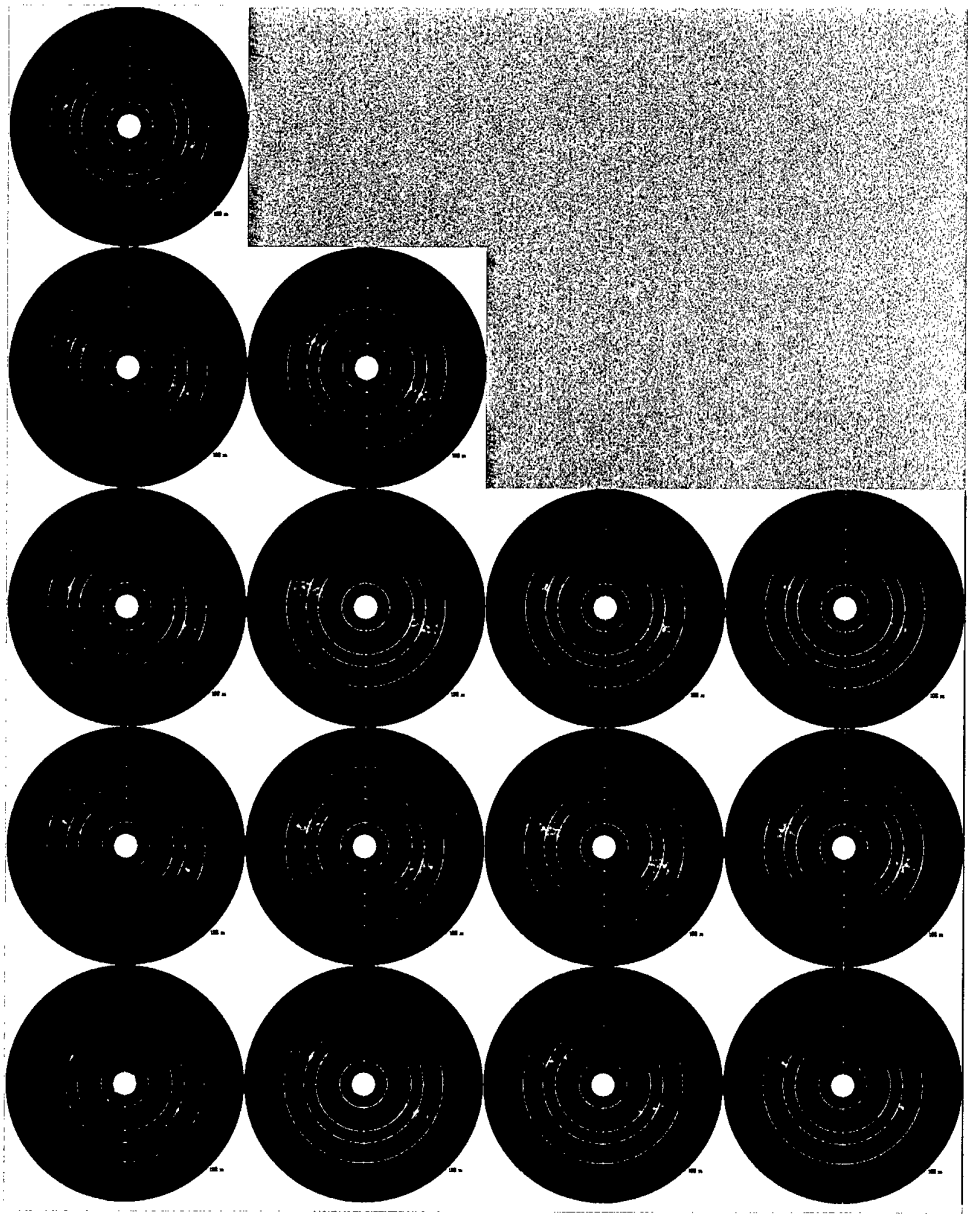

Figure 9 *High wave-number 2D-FFT spectra computed using 20 × 20 km blocks for March 3. The pink coloured peaks correspond to 200 m surface gravity waves.*

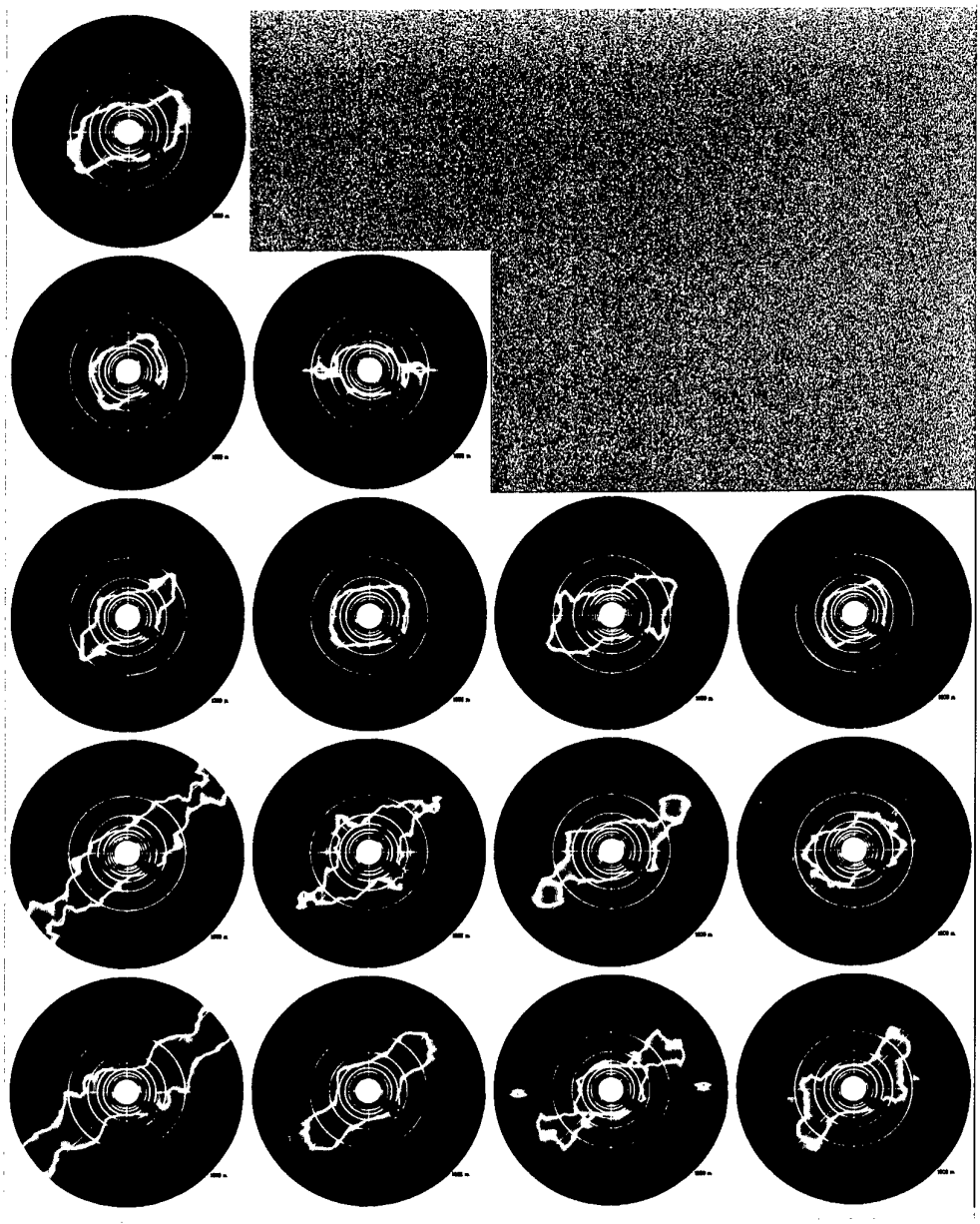

Figure 10 *Low wave-number 2D-FFT spectra computed using 20 × 20 km blocks for March 3. The green-blue coloured peaks correspond to 2 km waves.*

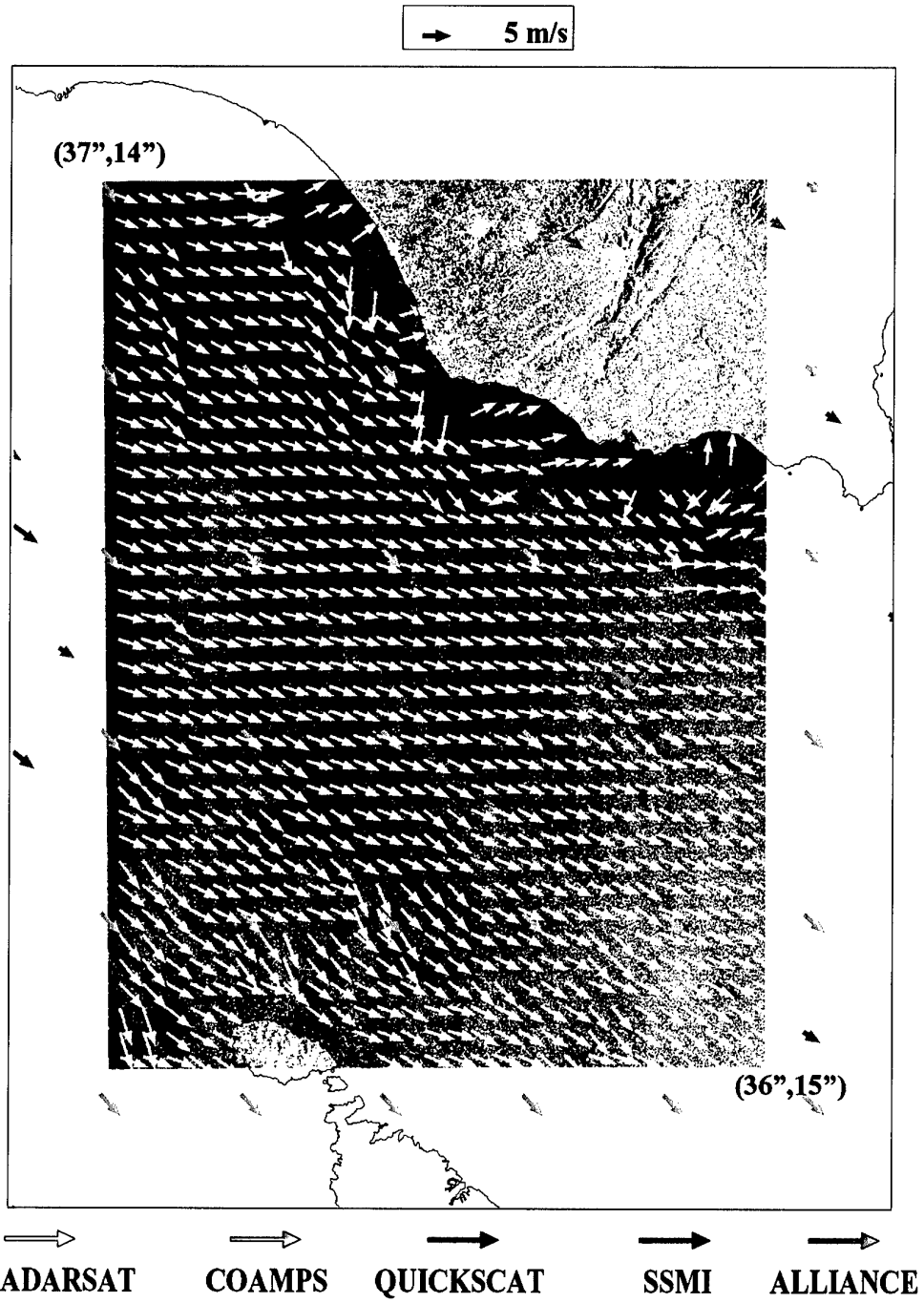

Figure 11 *Wind vector map for March 3 using wind-waves analysis*

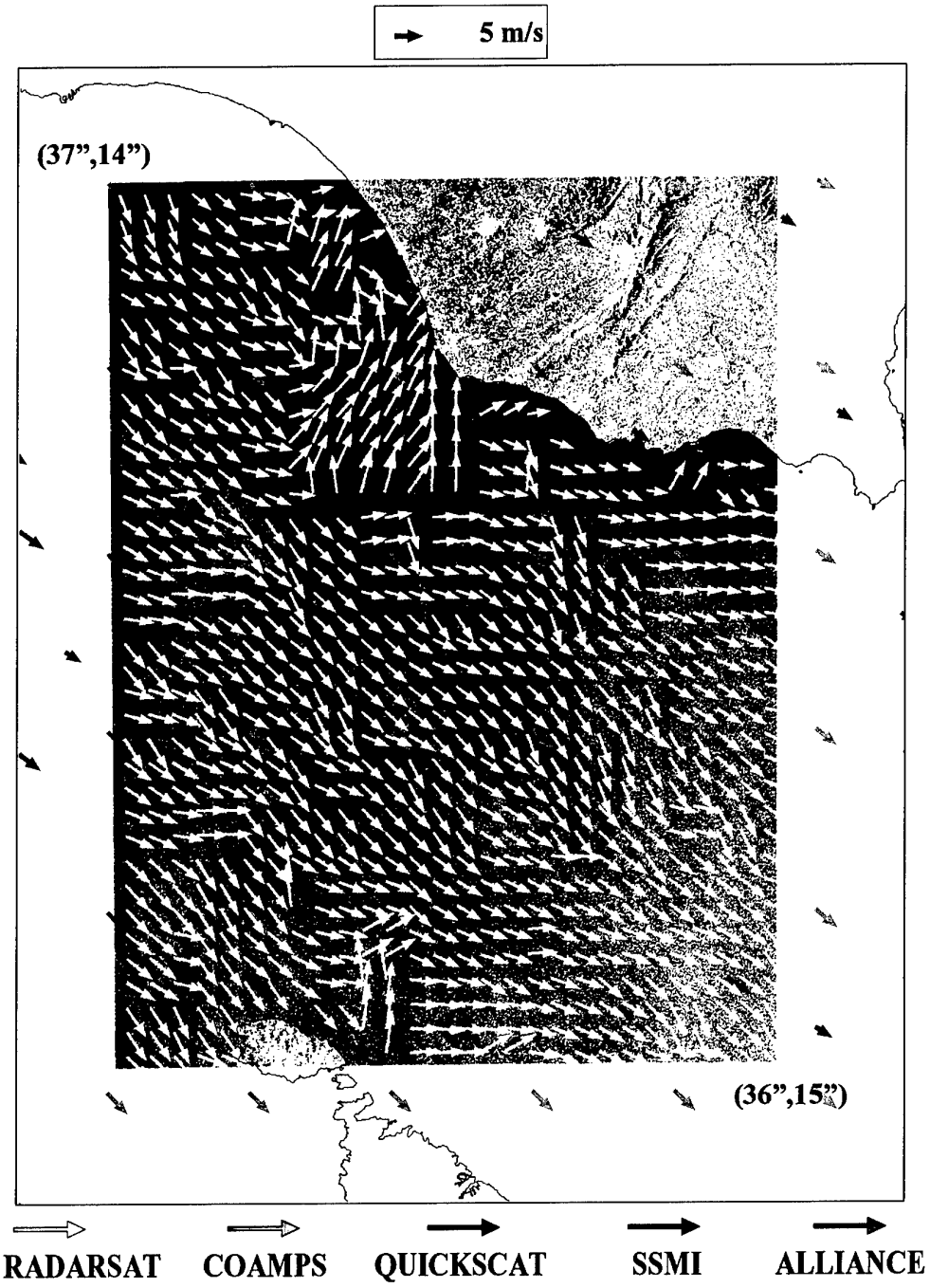

Figure 12 *Wind vector map for March 3 using wind-rolls analysis.*

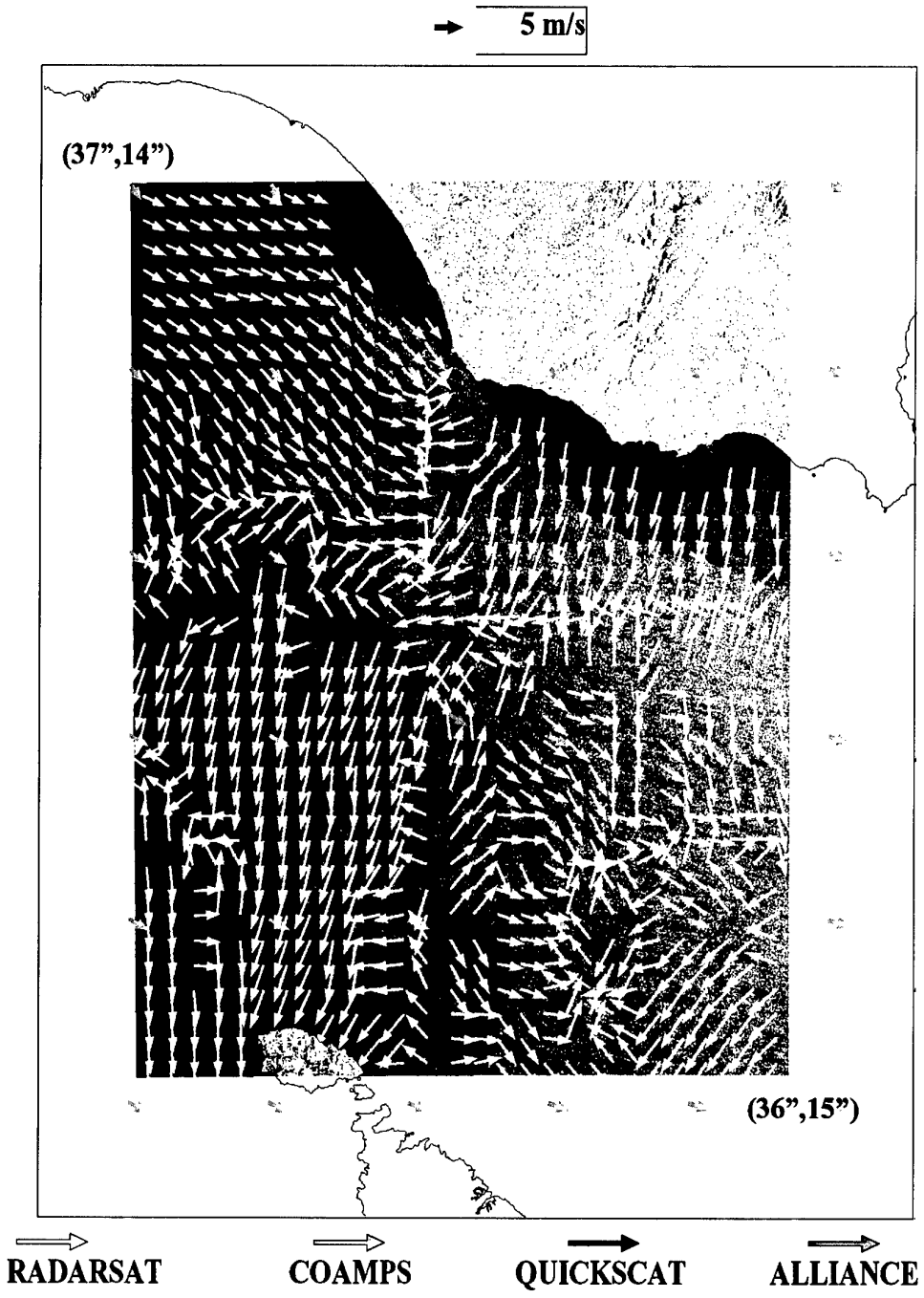

Figure 13 *Wind vector map for March 10 using wind-wave analysis.*

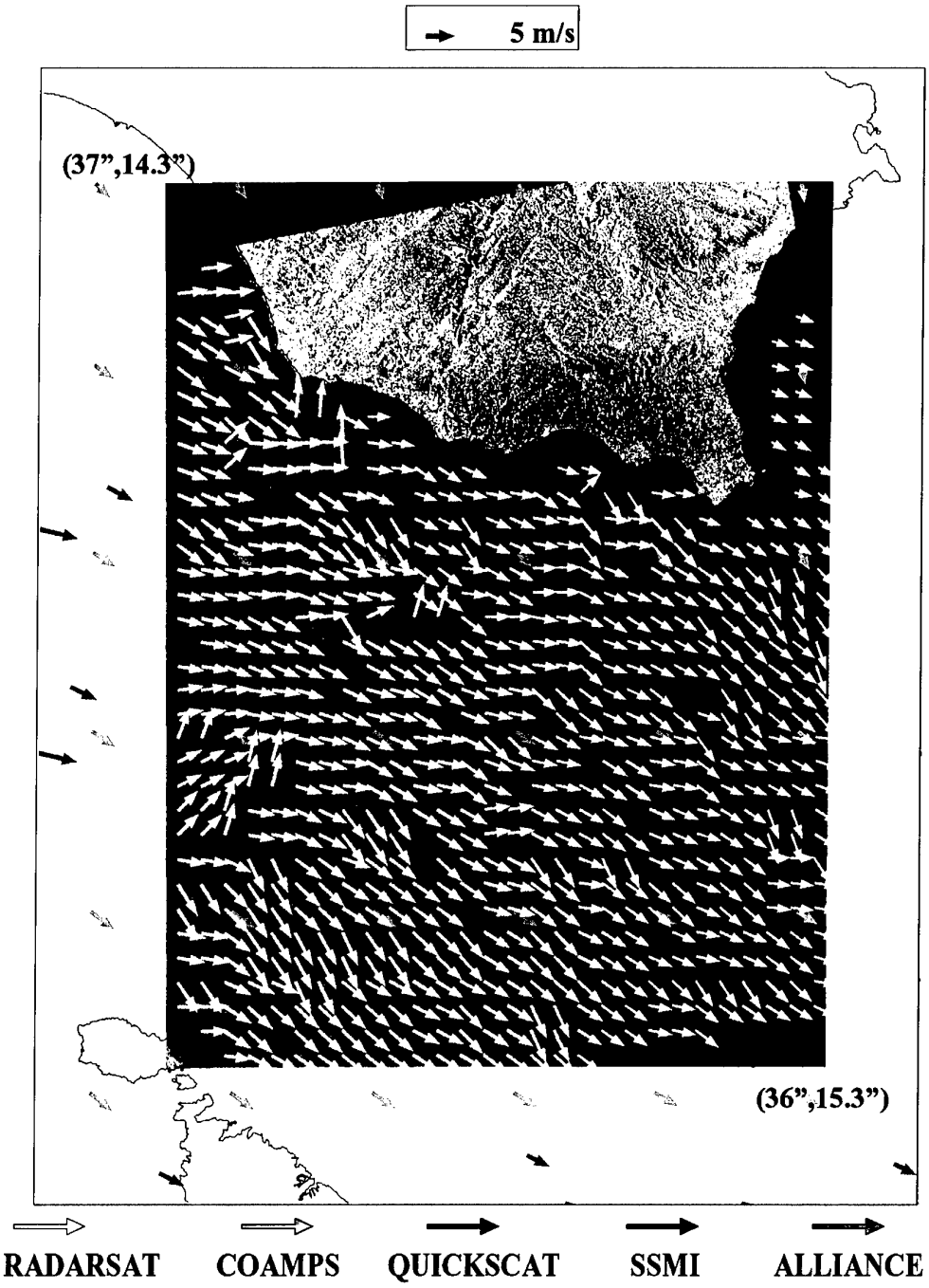

Figure 14 *Wind vector map for April 29 using wind-roll analysis.*

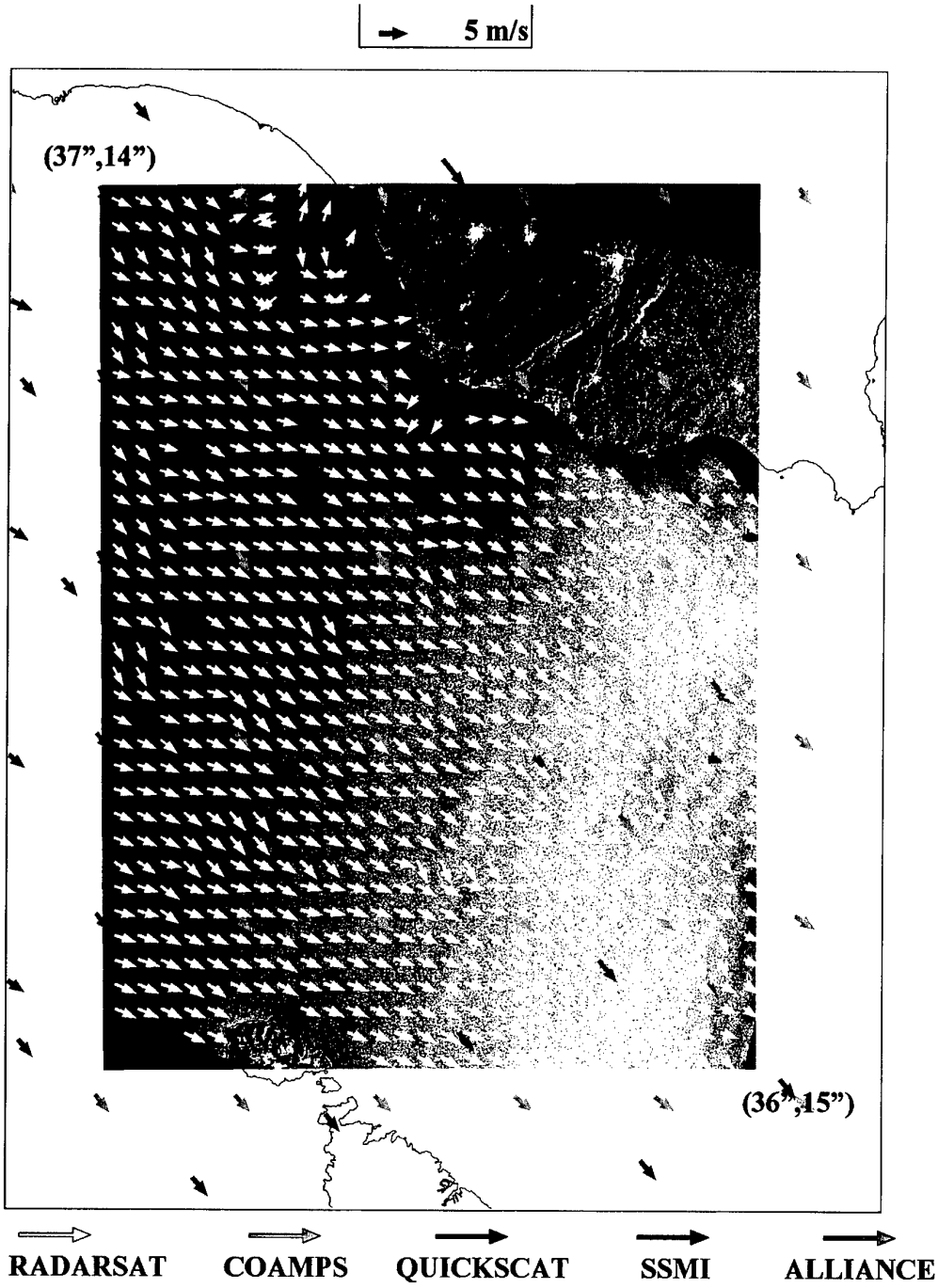

Figure 15 *Wind vector map for April 30 using wind-wave analysis.*

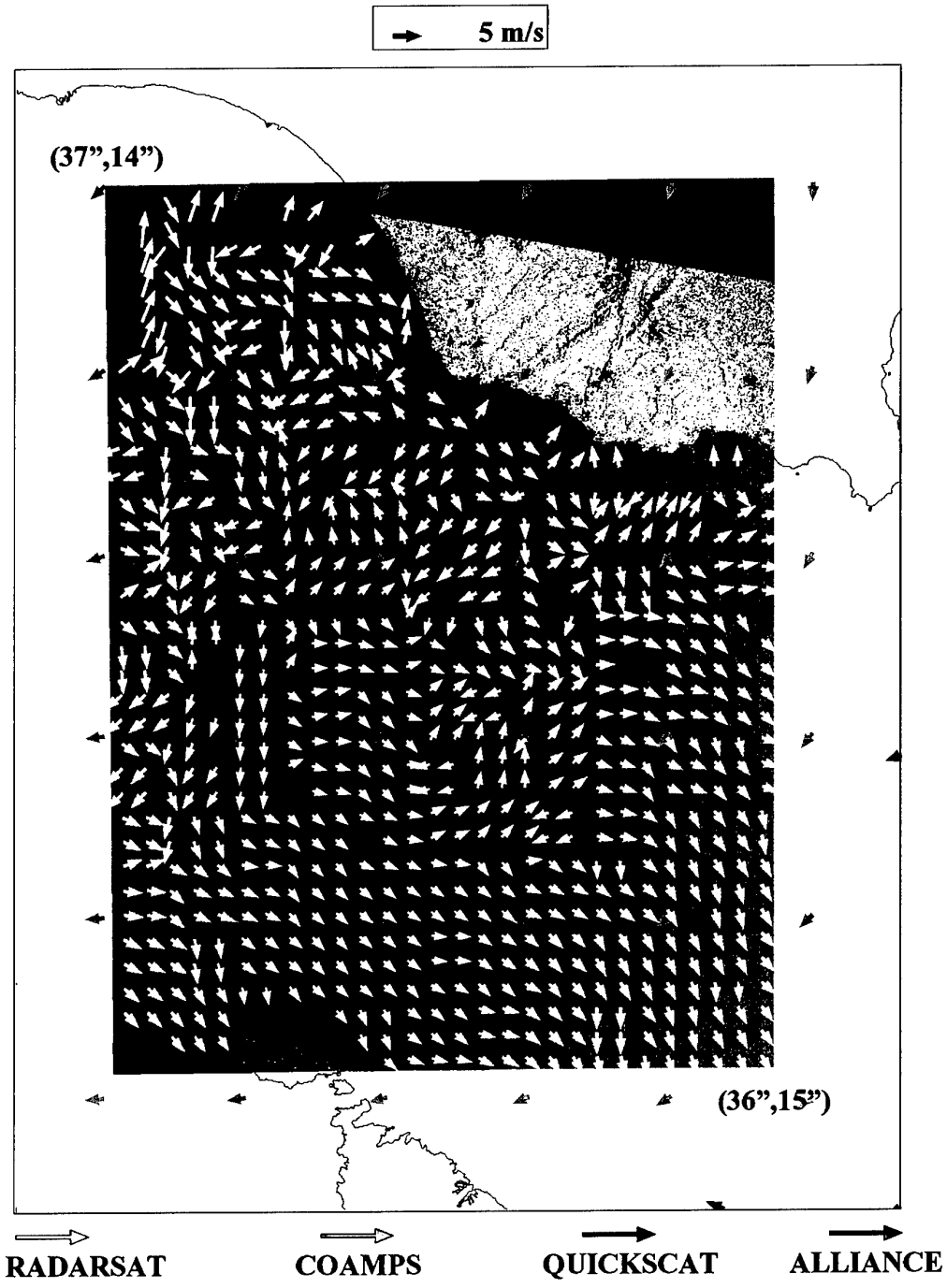

Figure 16 *Wind vector map for May 4 using wind-wave analysis.*

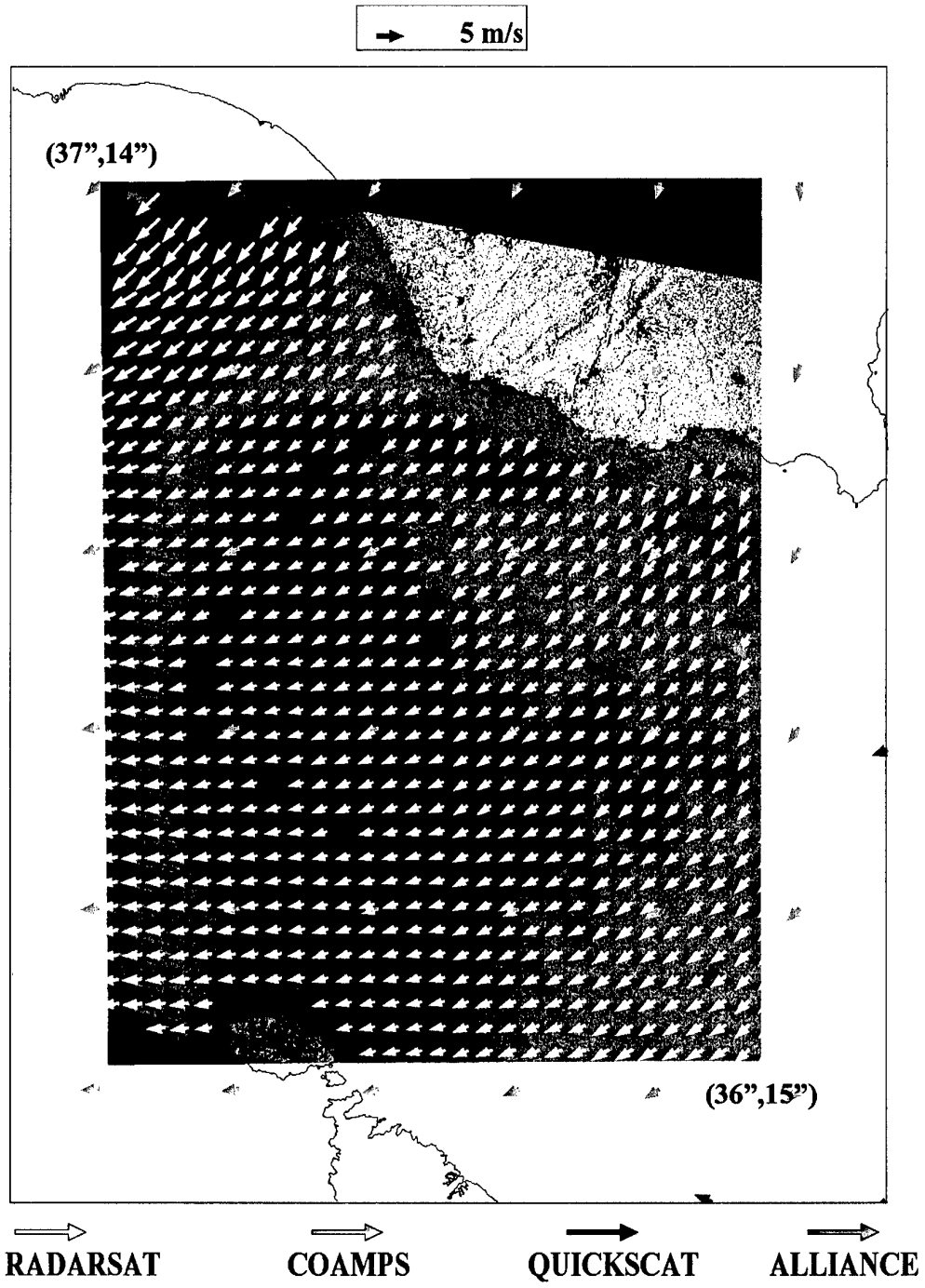

Figure 17 *Wind vector map for May 4 using COAMPS wind directions.*

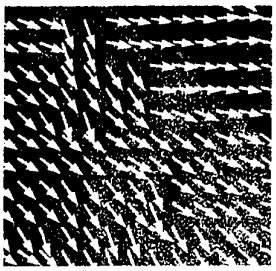

March 03 Streak Analysis

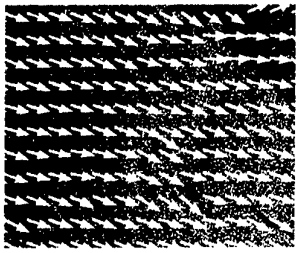

March 03 Wave Analysis

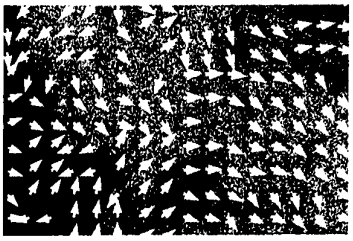

May04 Wave Analysis

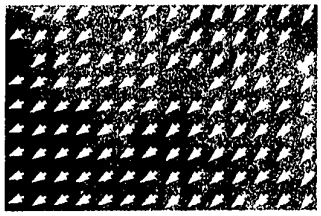

May04 COAMPS Analysis

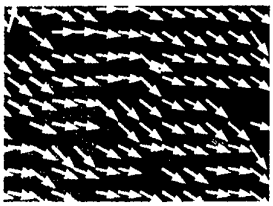

April 29 Streak Analysis

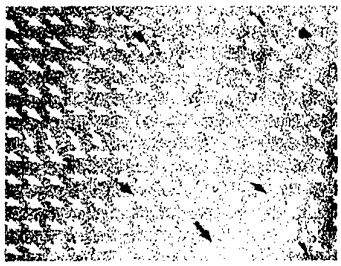

April30 Wave Analysis

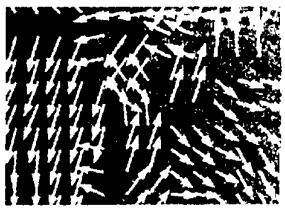

March 10 Wave Analysis

RADARSAT **COAMPS** **QUICKSCAT** **SSMI** **ALLIANCE**

Figure 18 *Comparative wind vector maps in the vicinity of* RV ALLIANCE.

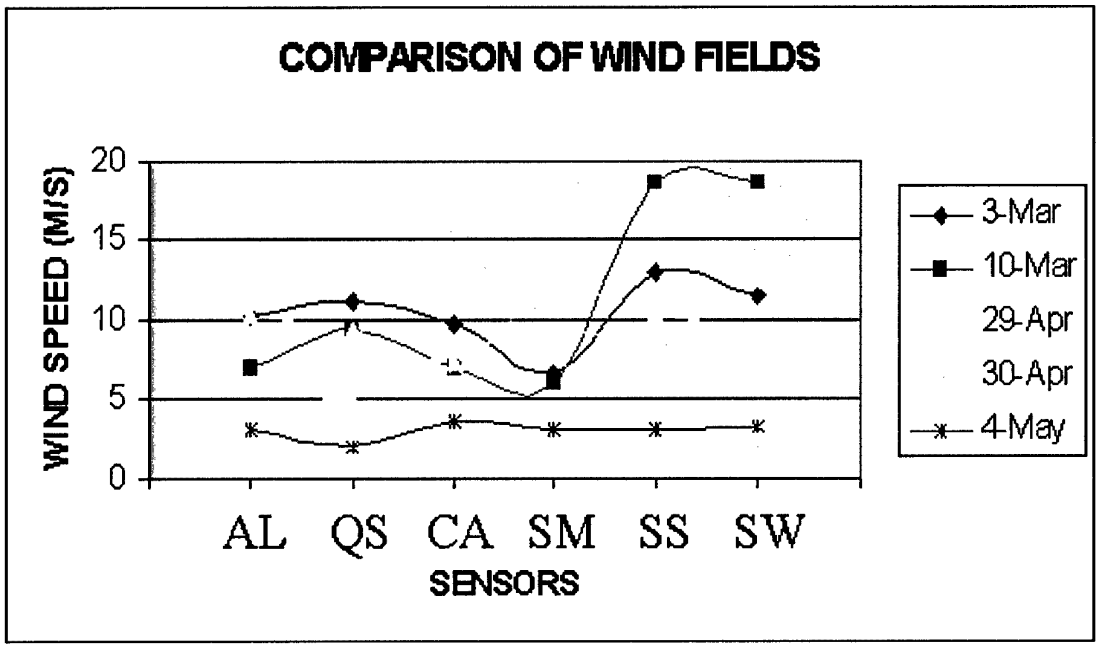

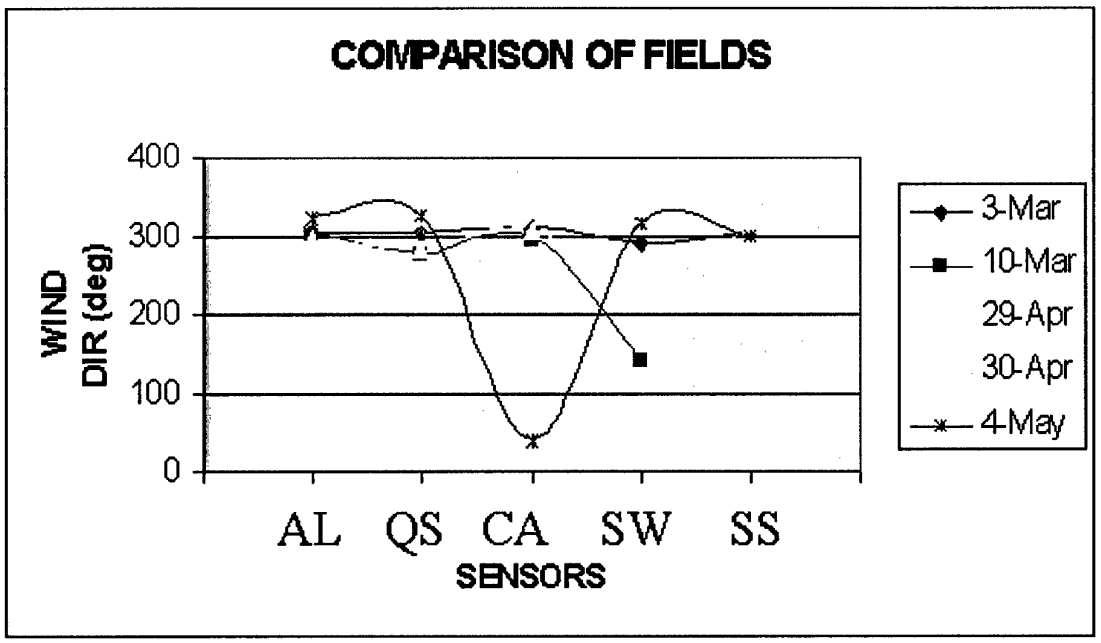

Figure 19 *2D plot of winds* vs *sensors. The symbols refer to AL: Alliance, QS:QUICKSCATT, SM: SSM/I, SS:SAR-WINDROLLS, SW:SAR-WIND-WAVES, respectively.*

Document Data Sheet

Security Classification		Project No.
UNCLASSIFIED		01-B
Document Serial No.	**Date of Issue**	**Total Pages**
SR-347	June 2001	37 pp.

Author(s)

Askari, F., Scevenels, S.

Title

High resolution wind mapping with RADARSAT SAR imagery

Abstract

This article assesses the capabilities of RADARSAT SAR imagery for high-resolution wind mapping. The mapping technique couples a scatterometer model function with two-dimensional image analysis and other fusion techniques for inverting the SAR back-scattering cross-sections into wind vectors. The SAR-derived results are compared with shipboard *in situ* measurements, coarse resolution winds derived from the coupled ocean atmosphere prediction system (COAMPS) model, special sensor microwave imager (SSM/I) and QUICKSCAT satellite measurements. The sensor-to-sensor comparisons show good overall agreement. The largest discrepancies are associated with measurements from the SCANSAR imaging mode, where antenna calibration is a suspect.

Keywords

Wind retrieval – scatterometry - RADARSAT

Issuing Organization

North Atlantic Treaty Organization
SACLANT Undersea Research Centre
Viale San Bartolomeo 400, 19138 La Spezia, Italy

[From N. America: SACLANTCEN (New York) APO AE 09613]

Tel: +39 0187 527 361
Fax:+39 0187 527 700

E-mail: library@saclantc.nato.int

The SACLANT Undersea Research Centre provides the Supreme Allied Commander Atlantic (SACLANT) with scientific and technical assistance under the terms of its NATO charter, which entered into force on 1 February 1963. Without prejudice to this main task - and under the policy direction of SACLANT - the Centre also renders scientific and technical assistance to the individual NATO nations.

This document is approved for public release.
Distribution is unlimited

SACLANT Undersea Research Centre
Viale San Bartolomeo 400
19138 San Bartolomeo (SP), Italy

tel: +39 0187 527 (1) or extension
fax: +39 0187 527 700

e-mail: library@saclantc.nato.int

NORTH ATLANTIC TREATY ORGANIZATION